Current Biology, Vol. 15, 214–225, February 8, 2005, ©2005 Elsevier Ltd All rights reserved. DOI 10.1016/j.cub.2005.01.038

The Mad1/Mad2 Complex as a Template for Mad2 Activation in the Spindle Assembly Checkpoint

Anna De Antoni,[1] Chad G. Pearson,[2,5] Daniela Cimini,[2] Julie C. Canman,[2,3] Valeria Sala,[1] Luigi Nezi,[1] Marina Mapelli,[1] Lucia Sironi,[1,4] Mario Faretta,[1] Edward D. Salmon,[2] and Andrea Musacchio[1,*]

[1]Department of Experimental Oncology
European Institute of Oncology
Via Ripamonti 435
20141 Milano
Italy

[2]Department of Biology
University of North Carolina at Chapel Hill
607 Fordham Hall
Chapel Hill, North Carolina 27599

Summary

Background: The spindle assembly checkpoint (SAC) imparts fidelity to chromosome segregation by delaying anaphase until all sister chromatid pairs have become bipolarly attached. Mad2 is a component of the SAC effector complex that sequesters Cdc20 to halt anaphase. In prometaphase, Mad2 is recruited to kinetochores with the help of Mad1, and it is activated to bind Cdc20. These events are linked to the existence of two distinct conformers of Mad2: a closed conformer bound to its kinetochore receptor Mad1 or its target in the checkpoint Cdc20 and an open conformer unbound to these ligands.

Results: We investigated the mechanism of Mad2 recruitment to the kinetochore during checkpoint activation and subsequent transfer to Cdc20. We report that a closed conformer of Mad2 constitutively bound to Mad1, rather than Mad1 itself, is the kinetochore receptor for cytosolic open Mad2 and show that the interaction of open and closed Mad2 conformers is essential to sustain the SAC.

Conclusions: We propose that closed Mad2 bound to Mad1 represents a template for the conversion of open Mad2 into closed Mad2 bound to Cdc20. This simple model, which we have named the "Mad2 template" model, predicts a mechanism for cytosolic propagation of the spindle checkpoint signal away from kinetochores.

Introduction

Before being divided into equal complements, sister chromatids attach to microtubules originating from opposite poles of the mitotic spindle (bipolar attachment). The SAC monitors this process and delays anaphase until all chromosomes have attained bipolar attachment [1, 2]. Spindle microtubules attach on kinetochores, protein scaffolds assembled on centromeric DNA [3]. The SAC senses kinetochore-microtubule attachment, and the tension between sister chromatids building up during this process [1, 2].

The SAC is conserved in all eukaryotes and includes mitotic arrest deficient (*MAD*) and budding uninhibited by benzimidazole (*BUB*) genes [1, 2]. Their products temporarily sequester Cdc20, an activator of the anaphase-promoting complex/cyclosome, the E3 ubiquitin ligase targeting securin and cyclin B for proteasome-mediated degradation. Destruction of securin activates separase, which triggers anaphase by cleaving the complex linking the sister chromatids, named Cohesin [4, 5]. The sequestration of Cdc20 requires Mad2 and BubR1 [1, 6]. Mad2 is a ~200 residue protein containing a Horma domain [7]. BubR1 consist of an N-terminal domain containing Bub3 and Cdc20 binding sites and a C-terminal kinase domain (missing in the budding yeast ortholog, Mad3) [1, 6]. Both Mad2 and BubR1 bind Cdc20 tightly, and their effects are synergic [8–13]. Consistently, Mad2, BubR1 (or Mad3), Bub3, and Cdc20 enter a single complex known as mitotic checkpoint complex (MCC) [11, 14–16].

Unattached kinetochores establish and maintain the SAC, and all SAC proteins show kinetochore localization in prometaphase [1, 3, 17]. Fluorescence recovery after photobleaching (FRAP) revealed stable kinetochore residents, including Bub1, Mad1, and a fraction of Mad2, and proteins with fast turnover at kinetochores, including Mad2, BubR1, Bub3, and Cdc20 [18–21]. These studies envision a stable catalytic platform at the kinetochore that senses lack of microtubule attachment and activates Mad2 and BubR1 to form the MCC with Cdc20 [1, 3, 6]. The exact composition of the MCC and the order of events subtending to its formation remain unclear (reviewed in [1, 6]). Mad2/Cdc20 and BubR1/Bub3/Cdc20 subcomplexes may form in subsequent or parallel steps with distinct dependencies. Here, we concentrate on the essential role of Mad1 in promoting binding of Mad2 to Cdc20, ignoring BubR1/Bub3, which is dispensable for this interaction [15, 22–25].

Mad1 is a 718 residue, predominantly coiled-coil protein whose N-terminal domain supports Mad2-independent binding to kinetochores in prometaphase [24, 26, 27]. The Mad1/Mad2 core complex is a tetrameric 2:2 assembly (Supplemental Figure S1) [28, 29]. Mad2 is recruited to the kinetochore thanks to its interaction with Mad1, and both proteins disappear from kinetochores upon microtubule attachment [12, 24, 26, 27, 30]. Because Mad1 and Mad2 are respectively stable and cycling at unattached kinetochores [18–21], Mad1 is believed to recruit Mad2 to kinetochores for exchange onto Cdc20.

Two aspects of Mad2 impinge upon this model. First, Mad1 and Cdc20 contain similar Mad2 binding motifs conforming to the consensus (K/R)$\phi\phi$XXXXXP (where

*Correspondence: andrea.musacchio@ifom-ieo-campus.it
[3]Present address: Institute of Molecular Biology, 1229 University of Oregon, Eugene, Oregon 97403.
[4]Present address: EMBL, Meyerhofstrasse 1, 69012 Heidelberg, Germany.
[5]Present address: University of Colorado at Boulder, Boulder, Colorado 80309.

ϕ is aliphatic, and X is any residue) that bind Mad2 in the same pocket [22, 29]. Second, Mad2 adopts two conformations, open Mad2 (O-Mad2, also known as N1-Mad2) and closed Mad2 (C-Mad2, or N2-Mad2), differing for a structural change in the "safety belt," the 50 residue C-terminal segment of Mad2 (Supplemental Figure S1) [22, 29, 31, 32]. Mad2 adopts the closed conformation when bound to Cdc20 or Mad1 and the open conformation when unbound to these ligands [22, 29, 31–33]. Because a large energy barrier separates the O- and C-Mad2 conformers [29, 32], the conformational transition may be rate limiting for the ability of Mad2 to bind Cdc20 and ultimately for SAC activation. Thus, it is essential to understand the role of Mad1 in this transition.

We investigated how Mad1 recruits Mad2 from the cytosol to the kinetochore and discovered that C-Mad2 stably bound to Mad1, rather than Mad1, constitutes the kinetochore receptor of O-Mad2. After being recruited, O-Mad2 is converted into C-Mad2 bound to Cdc20. Although we do not provide direct insight into how Mad1 bound C-Mad2 favors the conversion of O-Mad2 into Cdc20 bound C-Mad2, we show that the interaction between Mad1 bound C-Mad2 and O-Mad2 is essential to maintain the SAC. In our interpretation, Mad1/Mad2 is a template for the formation of a structurally equivalent Cdc20/Mad2 copy that amplifies the SAC signal away from kinetochores.

Results

Testing the "Mad2 Exchange" Model

In the recently proposed "Mad2 exchange" model [32], Mad1 lowers the energy barrier for the transition of O-Mad2 into C-Mad2 by recruiting O-Mad2 to kinetochores, changing its conformation to C-Mad2 and releasing it as C-Mad2 for Cdc20 binding (Figure 1A). We decided to test the assumption of this model that Mad1/Mad2 functions as a source of Mad2 in the presence of Cdc20. In preliminary control experiments, we studied the interaction of $Mad2^{wt}$ with Cdc20 in the absence of Mad1. Although Mad2 binding to Cdc20 requires Mad1 in vivo, it spontaneously occurs in vitro [22–24, 28]. We compared the elution profiles of $Mad2^{wt}$ from a Superdex-200 PC 3.2/30 size-exclusion chromatography (SEC) column with that of an incubation of Mad2 with Cdc20 (Figures 1B and 1C). In agreement with previous reports, the elution volume (V_E) of Mad2 (1.55 ml) was typical of an oligomer [22, 28, 31, 34]. As explained below, Mad2 forms oligomers thanks to the interaction of its two conformers, O-Mad2 and C-Mad2. Bacterially expressed $Mad2^{wt}$ dimerizes because a fraction of O-Mad2 spontaneously converts into empty C-Mad2 (i.e., devoid of Mad1 or Cdc20), which binds the residual fraction of O-Mad2 [32, 33].

$Mad2^{wt}$ (40 μM) was incubated for 1 hr with a 10-fold excess of a synthetic peptide encompassing residues 111–138 of Cdc20 ($Cdc20^{111–138}$), a stronger Mad2 ligand than full-length Cdc20 [9, 35], to generate Mad2/Cdc20. After SEC, a single $Mad2^{wt}$ peak was present whose V_E (1.65 ml, Figure 1C) indicated a 1:1 $Mad2^{wt}/Cdc20^{111–138}$ complex. The shift in V_E relative to apo-$Mad2^{wt}$ (the Cdc20 peptide does not significantly contribute to the Stokes radius of the complex) demonstrates that $Cdc20^{111–138}$ binds Mad2 and that pure C-Mad2 created by $Cdc20^{111–138}$ does not form Mad2 dimers, as shown previously [22, 28].

Next, we asked if $Cdc20^{111–138}$ caused the release of $Mad2^{wt}$ from Mad1/Mad2. The isolated $Mad1^{485–718}/Mad2^{wt}$ core complex eluted as a single peak with an apparent molecular weight (MW) of 180 kDa (Figure 1D). The elongated shape of Mad1/Mad2 likely explains deviation from the expected MW ($\sim$110 kDa) because the 2:2 stoichiometry is known from structural analysis [29] and analytical ultracentrifugation (not shown). When Mad1/Mad2 (20 μM, tetramer concentration) was incubated with a 10-fold excess of $Cdc20^{111–138}$ and analyzed by SEC (Figure 1E), we did not observe significant shifts in the V_E of Mad1/Mad2 nor the release of Mad2 or Mad2/Cdc20, as already reported [28, 29]. Thus, it cannot be assumed that Mad2 dissociates from Mad1 to bind Cdc20. Despite similar Mad2 binding affinities of the Mad1 and Cdc20 motifs (Supplemental Table S1 and [29]), Mad1/Mad2 is strongly stabilized by tetramerization, explaining why Cdc20 does not remove Mad2 from Mad1/Mad2 [28, 29].

In the "Mad2 exchange" model Mad1 and Cdc20 bind the same Mad2 pocket. Even if under appropriate conditions Mad1/Mad2 dissociated to release Mad2 for Cdc20, Mad1 should be viewed as a competitive inhibitor of Mad2/Cdc20 rather than a catalyst as proposed [32]. To show this, we studied how the Mad2 binding segment of Mad1 ($Mad1^{527–555}$) influenced Mad2 binding to Cdc20. If Mad1 catalyzed this interaction, on a time course, one should observe at least equal but possibly larger amounts of Cdc20 bound Mad2 in the presence of Mad1 than in its absence. In the presence of increasing amounts of $Mad1^{527–554}$ peptide, Mad2 (3 μM) was incubated with GST-$Cdc20^{111–138}$ (1.4 μM) preabsorbed onto glutathione-Sepharose (GSH) beads. At different times, the beads were collected, washed, and the amount of bound Mad2 was evaluated (Figure 1F). In all experiments, we observed inhibition of Mad2 binding to Cdc20 that increased with the concentration of $Mad1^{527–554}$. This confirms that direct exchange of Mad2 from Mad1 to Cdc20 implicates Mad1 and Cdc20 as competitors, contradicting the proposition that Mad1 catalyses formation of Mad2/Cdc20 [32]. Consistently, overexpression of the Mad2 binding region of Mad1 abrogates the SAC likely because Mad2 engages in a complex with Mad1 that prevents it from binding Cdc20 [22, 24, 36]. Although this does not prove the "Mad2 exchange" model wrong, it proves it inadequate to explain the requirements for fast activation of Mad2 for Cdc20 binding (the model is further discussed in Supplemental Figures S2 and S3).

Mad1/Mad2 Binds Mad2 In Vitro

Knowing that Mad1 mediates kinetochore localization of Mad2 and that Mad1/Mad2 is stable, we hypothesized that Mad1/Mad2, rather than Mad1, is the Mad2 receptor. To test this, we labeled $Mad2^{wt}$ covalently with Alexa Fluor 488 (abbreviated in Alexa) and compared the SEC elution profiles of Alexa-modified Mad2 (40 μM) before or after adding stoichiometric amounts of Mad1/Mad2 (20 μM of divalent tetramer). Alexa-$Mad2^{wt}$ eluted as an

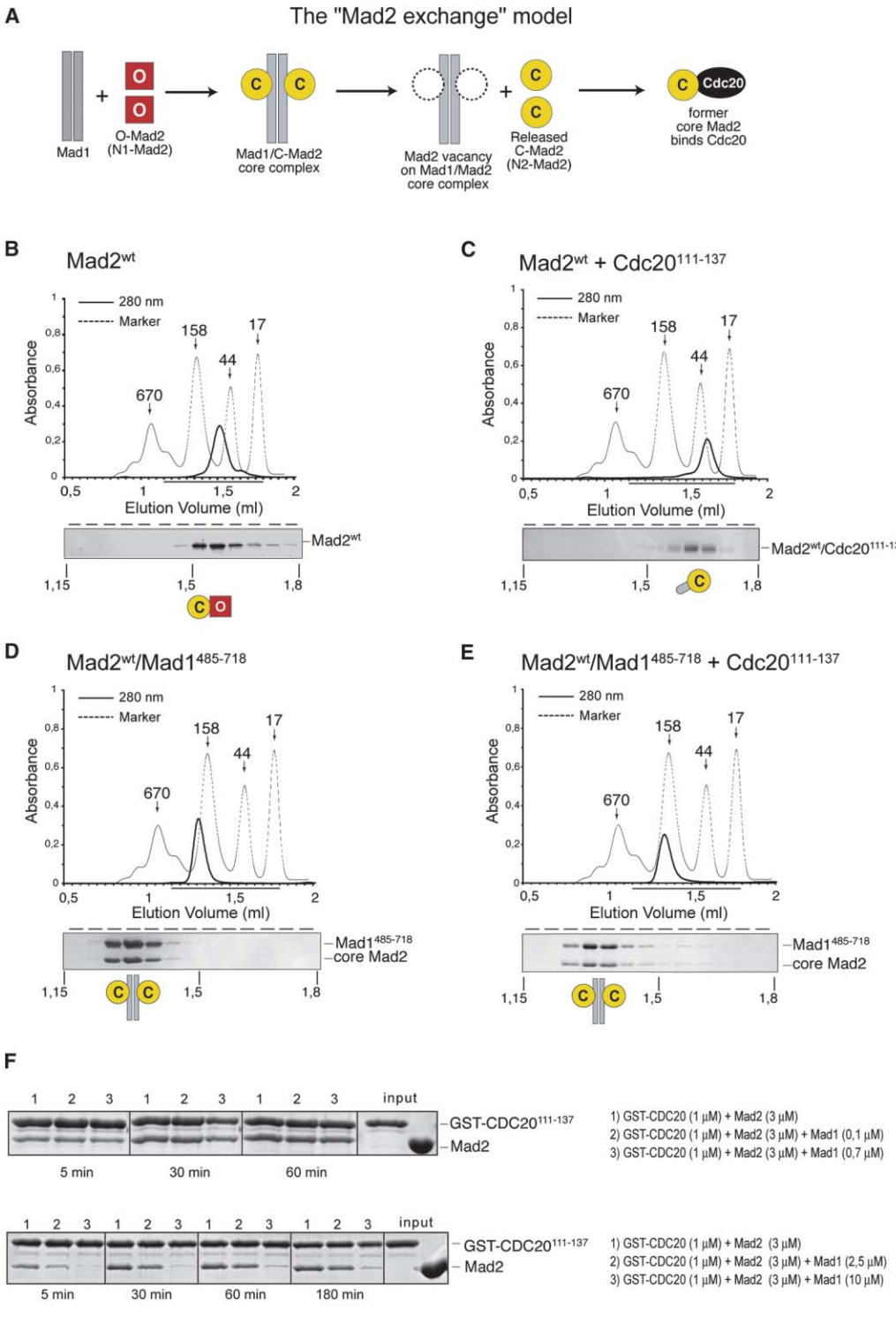

Figure 1. Testing the "Mad2 Exchange" Model

(A) The "Mad2 exchange" model predicts that Mad1 binds O-Mad2 (defined N1-Mad2 in [29] and displayed as a red square), generating the Mad1/Mad2 core complex (gray and yellow, respectively). This releases C-Mad2 (N2-Mad2 in [29] and displayed as a yellow circle) for Cdc20, leaving a vacancy on Mad1 filled by O-Mad2.

(B) SEC elution profile of Mad2^{wt}. All 50 µl fractions spanning from 1.15 to 1.8 ml were separated by SDS-PAGE and stained with Coomassie.

(C) After incubating with Cdc20$^{111-138}$, Mad2^{wt} is turned into C-Mad2 and elutes as a 1:1 Mad2/Cdc20 complex. The Cdc20 peptide eluted after the 2 ml mark.

(D) Elution profile of purified recombinant Mad1$^{485-718}$/Mad2^{wt} core complex.

(E) When incubated in vitro with Cdc20$^{111-138}$, the core complex remains intact and does not release free Mad2/Cdc20.

(F) GST-Cdc20$^{111-138}$ bound to GSH beads was incubated with Mad2^{wt} with or without Mad1$^{527-554}$. Beads were washed, and bound proteins were identified by Coomassie staining after SDS-PAGE.

oligomer (Figure 2B) (green trace reports Alexa absorbance at 495 nm). When incubated for 1 hr with Mad1/Mad2, most Mad2^{wt} entered a high MW complex coeluting with Mad1/Mad2 (Figure 2C). Cdc20$^{111–138}$ fails to dissociate Mad1/Mad2 (Figure 1E). Conversely, when the complex of Alexa-Mad2^{wt} with Mad1/Mad2 was treated with a 10-fold excess of Cdc20$^{111–134}$, most Alexa-Mad2^{wt} dissociated from Mad1/Mad2 and eluted with the MW of Mad2/Cdc20$^{111–134}$ (Figure 2D). Thus, Alexa-Mad2^{wt} binds Mad1/Mad2 differently from the core subunits, which are insensitive to Cdc20$^{111–134}$ (Figure 1E). Because Alexa-Mad2^{wt} bound to Cdc20 has the C-Mad2 conformation, this experiment suggests that C-Mad2 is unable to bind Mad1/Mad2.

To corroborate these conclusions, we turned to Mad2 mutants with selectively altered functions (Table 1 and Supplemental Figure S4). Mad2$^{\Delta C}$ is unable to bind Mad1 or Cdc20 because a 10-residue C-terminal deletion locks the safety belt in the O-Mad2 conformation (Supplemental Figure S1) [29, 31]. We confirmed this with many new experiments (Supplemental Figure S5 and Supplemental Table S1). In SEC experiments, Alexa-Mad2$^{\Delta C}$ eluted as a monomer (Figure 2E), showing that pure O-Mad2, like pure C-Mad2, does not form dimers. Like Alexa-Mad2^{wt}, Alexa-Mad2$^{\Delta C}$ entered a stoichiometric complex with Mad1/Mad2 (Figure 2F). As expected, however, Cdc20$^{111–138}$ did not dissociate Mad2$^{\Delta C}$ from Mad1/Mad2 (Figure 2G). Because Mad2$^{\Delta C}$ is unable to form a core complex with Mad1 and Mad1 contains a single Mad2 binding site [22, 28, 29] (R. Hagan et al., submitted), we conclude that Mad1 binding is not required to recruit Mad2 onto the Mad1/C-Mad2 complex and that the recruited subunits are noncore ("external"). Furthermore, the results confirm that "external" Mad2 is recruited onto the Mad1/Mad2 as O-Mad2, the conformation of Mad2$^{\Delta C}$.

Mad2$^{R133E-Q134A}$ Fails to Bind Mad1/Mad2

In summary, O-Mad2 binds (1) C-Mad2 in the Mad1/Mad2 complex, (2) C-Mad2 generated with the Mad2 binding motifs of Mad1 or Cdc20 (Supplemental Table S1, Supplemental Figure S5, and data not shown), and (3) C-Mad2 spontaneously forming in bacterial preparations of Mad2, causing its oligomerization [33]. Mutations impairing the O-Mad2/C-Mad2 binding interface should prevent Mad2 oligomerization. If such mutations did not affect the potential of Mad2 to convert from O- to C-Mad2, the ability to bind Mad1 and Cdc20 would be retained. Mad2^{R133A} is a monomeric mutant that binds tightly to Mad1 and Cdc20 and whose bacterial preparations contain both O-Mad2 and C-Mad2 [28, 29, 32]. Confirming our expectation, Alexa-Mad2^{R133A} bound poorly to the Mad1/Mad2 complex [33]. To obtain a more penetrant phenotype, we created the double mutant Mad2$^{R133E-Q134A}$ (the Mad2$^{R133A-Q134A}$ mutant was insoluble). Binding of Alexa-Mad2$^{R133E-Q134A}$ to Mad1/Mad2 was impaired (Figures 2H–2I). In solution and solid phase, Mad2$^{R133E-Q134A}$ bound Mad1 and Cdc20 as effectively as Mad2^{wt} (Supplemental Table S1 and Supplemental Figure S5). R133 and Q134 are invariant in all Mad2 orthologs [7], indicating that the binding function they mediate is conserved in evolution. Mad2$^{\Delta C}$ and Mad2$^{R133E-Q134A}$ have complementary properties. Mad2$^{\Delta C}$ fails to bind Mad1 and Cdc20 but retains the ability to bind C-Mad2 (Figure 2F and Table 1). Mad2$^{R133E-Q134A}$ binds Mad1 and Cdc20, but its open conformer fails to bind C-Mad2 (Figure 2I, Table 1, Supplemental Figure S5, and data not shown).

Mad1/Mad2 Is the Kinetochore Receptor of Mad2

We asked if our results in vitro correlated with the ability of the same Alexa-Mad2 species to bind the endogenous Mad2 receptor at kinetochores. Early prometaphase PtK1 cells were microinjected with 1%–5% cell volume of Alexa-labeled Mad2^{wt}, Mad2$^{\Delta C}$, Mad2$^{R133E-Q134A}$, or Mad2$^{\Delta C-R133E-Q134A}$ (typically at needle concentrations of 3 μM) and analyzed by live cell fluorescence microscopy. Imaging was started $\sim$20 min after injection and continued for $\sim$30 min. Out of 28 cells injected with Alexa-Mad2^{wt}, 26 showed strong kinetochore localization at unattached kinetochores of chromosomes that had not congressed to the spindle equator, as previously described [18], and only two showed weak localization (Figure 3A).

As Alexa-Mad2^{wt}, also Alexa-Mad2$^{\Delta C}$ displayed kinetochore localization at unattached kinetochores in 29 out of 31 injected cells (Figure 3B). The Alexa-Mad2$^{R133E-Q134A}$ double mutant, on the other hand, failed to localize to the kinetochore in 22 of 23 injected prometaphase Ptk1 cells with only one dimly positive cell (Figure 3C) in agreement with its inability to interact with the Mad1/Mad2 complex in vitro. To show that Mad2$^{\Delta C}$ uses the interface containing Arg133 and Gln134 to localize to kinetochores, we injected Alexa-labeled Mad2$^{R133E-Q134A-\Delta C}$ triple mutant in PtK1 cells. As expected, Mad2$^{R133E-Q134A-\Delta C}$ was unable to localize to the kinetochore in all 17 injected cells (Figure 3D), confirming that O-Mad2 (elicited by the ΔC deletion) requires Arg133 and Gln134 to bind its endogenous kinetochore receptor. The coincidence of results with Mad2^{wt}, Mad2$^{\Delta C}$, Mad2$^{R133E-Q134A}$, and Mad2$^{R133E-Q134A-\Delta C}$ in vitro and in living demonstrates that the Mad1/Mad2 core complex, rather than Mad1, is the kinetochore receptor for Mad2. Our results confirm that Mad2 is recruited to kinetochores as O-Mad2. Furthermore, lack of kinetochore recruitment of an excellent Mad1 ligand such as Mad2$^{R133E-Q134A}$ suggests that there are no Mad2 vacancies on kinetochore Mad1 and that Mad1/Mad2 is stable during checkpoint activation.

Functional Analysis of Mad2$^{\Delta C}$

Mad2$^{\Delta C}$ has a dominant-negative (DN) effect on the SAC [12, 32, 36, 37]. As shown in Figure 4A, this effect can be explained by the binding of Mad2$^{\Delta C}$ to Mad1/Mad2, which creates an unproductive complex antagonizing the transfer of endogenous O-Mad2 to Cdc20. Consistent with this idea, Cdc20$^{111–138}$ releases Mad2^{wt} preloaded onto the Mad1/Mad2 core complex (Figure 2D), but not Mad2$^{\Delta C}$ (Figure 2G). For confirmation of the previous observations, HeLa cells were transfected with pCMV vectors expressing myc-tagged Mad2^{wt} or Mad2$^{\Delta C}$ to test the effects of their overexpression on the SAC (Figure 4B). 28–30 hr after transfection, half of the culture was incubated with nocodazole to activate the SAC. 18 hr later, the cells were harvested and

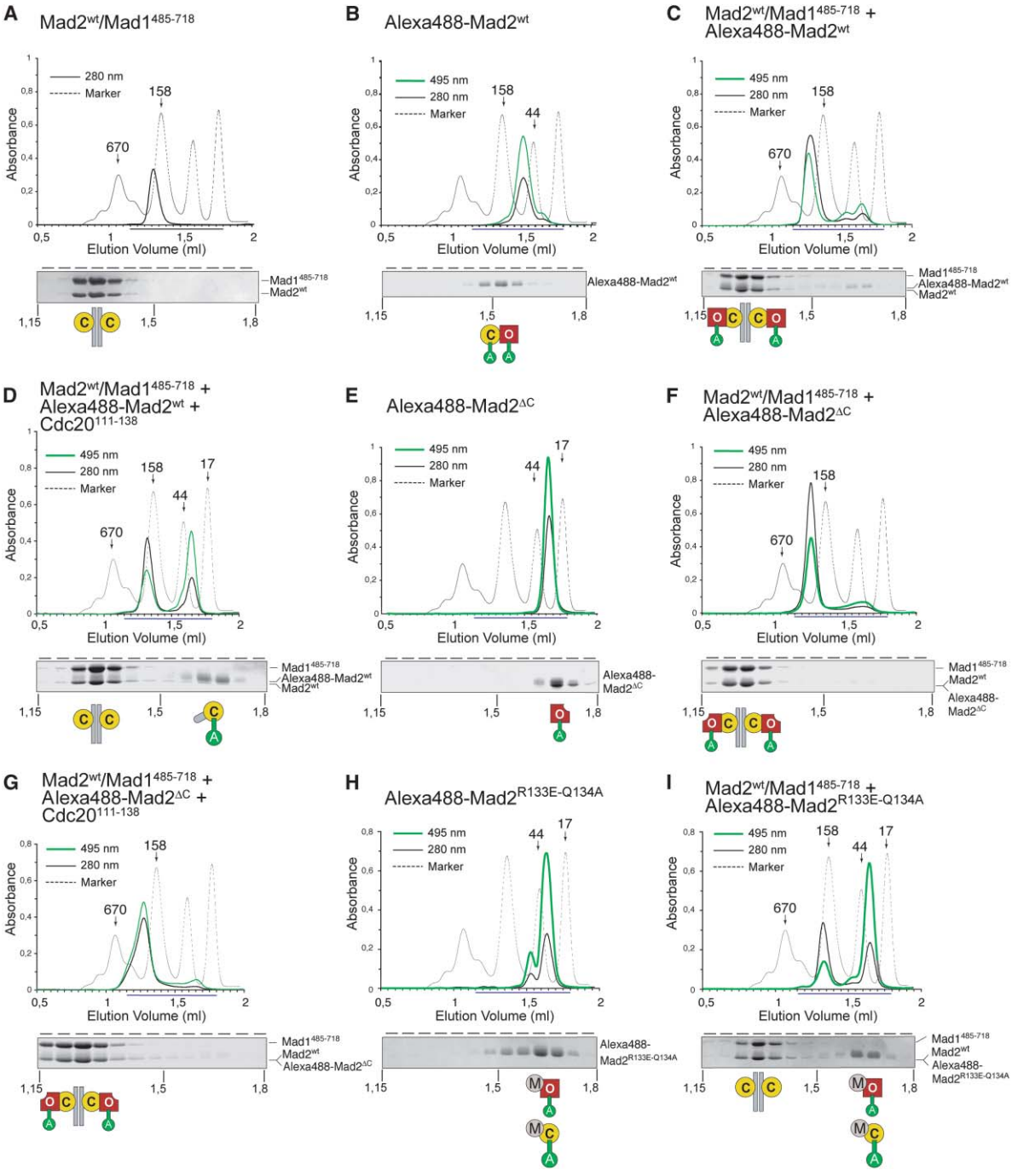

Figure 2. The Mad1/Mad2 Core Complex Binds O-Mad2

SDS-PAGE and Coomassie staining of the content of thirteen 50 μl fractions eluting between 1.15 and 1.8 ml. Traces recorded at 280 nm and 495 nm are black and green, respectively. A green bulb on Mad2 squares and circles indicates Alexa modification. (A) Elution profile of the Mad1$^{485–718}$/Mad2^{wt} core complex, already shown in Figure 1B. (B) Profile of Alexa-Mad2^{wt}. (C) SEC profile of Alexa-Mad2^{wt} mixed with stoichiometric amounts of Mad1$^{485–718}$/Mad2^{wt} core. Mad2^{wt} is made of O-Mad2/C-Mad2 dimers, but only O-Mad2^{wt} binds Mad1/Mad2. C-Mad2 and O-Mad2 interconvert rather rapidly. During a 1 hr incubation, most C-Mad2 is converted into O-Mad2, which then binds Mad1/Mad2, explaining why the majority of Mad2^{wt} is incorporated onto the Mad1/Mad2 complex. (D) As in (C), after addition of Cdc20$^{111–138}$. The majority of Alexa-Mad2^{wt} is released from the Mad1/Mad2 core in complex with Cdc20$^{111–138}$. (E) Elution profile of Alexa-Mad2^{ΔC}. (F) Profile of stoichiometric amounts of Alexa-Mad2^{ΔC} mixed with Mad1$^{485–718}$/Mad2^{wt} core. (G) Addition of Cdc20$^{111–138}$ to Alexa-Mad2^{ΔC} bound to Mad1/Mad2 core complex. Alexa-Mad2^{ΔC} does not dissociate in the presence of Cdc20$^{111–138}$. (H) Elution profile of Alexa-Mad2$^{R133E-Q134A}$. (I) Profile of Alexa-Mad2$^{R133E-Q134A}$ incubated stoichiometrically with the Mad1/Mad2 core complex.

Table 1. Properties of Mad2 and Mad2 Mutants

Mad2 Allele	Mutation	Effect	Conformation Allowed	Mad1 or Cdc20 Binding	Binding to Core Complex	Most Relevant References for Mutant
$Mad2^{wt}$	None	Not applicable	O-Mad2 C-Mad2	Yes	Yes	
$Mad2^{\Delta C}$	10 residue C-terminal deletion	Prevents conversion of C-terminal tail into closed position.	O-Mad2	No	Yes	[28, 31, 32, 34, 36]
$Mad2^{R133A}$	Arg133 to Ala	Prevents interaction of open form with closed form in a pure preparation. Residual binding to opposite conformers of $Mad2^{wt}$ was observed.	O-Mad2 C-Mad2	Yes	Weak	[28, 32, 40]
$Mad2^{R133E-Q134A}$	Arg133 to Glu Gln134 to Ala	Prevents interaction of open form with closed form with increased penetrance relative to $Mad2^{R133A}$.	O-Mad2 C-Mad2	Yes	No	This study
$Mad2^{R133E-Q134A-\Delta C}$	Arg133 to Glu Gln134 to Ala 10 residue C-terminal deletion	Prevents interaction of open form with closed form and conversion of C-terminal tail into closed position.	O-Mad2	No	No	This study

mitotic cells identified by flow cytometry for containing replicated (4N) DNA and phosphorylated histone H3 (H3-P, a mitotic marker, Figure 4C). In the absence of nocodazole, overexpression of $Mad2^{wt}$ caused strong accumulation of mitotic cells (Figure 4C, left), indicating that $Mad2^{wt}$ overexpression activates the SAC in HeLa cells. Cells overexpressing $Mad2^{\Delta C}$ did not arrest in mitosis in the absence of nocodazole, indicating that high levels of this mutant are unable to trigger the SAC. In the presence of nocodazole, HeLa cells transfected with an empty pCMV vector or overexpressing $Mad2^{wt}$ arrested in mitosis, whereas $Mad2^{\Delta C}$-expressing cells failed to arrest, indicating that they are checkpoint defective (Figure 4C, right). Overexpression of $Mad2^{R133A-\Delta C}$ did not perturb cell cycle progression in the absence of nocodazole and did not impair the SAC in nocodazole (Figure 4C). Because $Mad2^{\Delta C}$ differs from $Mad2^{R133A-\Delta C}$ only for the ability to bind Mad1/Mad2, we conclude that the DN effect of $Mad2^{\Delta C}$ on the SAC requires C-Mad2 binding.

Functional Analysis of $Mad2^{R133A}$ and $Mad2^{R133E-Q134A}$

If the interaction between O-Mad2 and Mad1/Mad2 were essential for the SAC, physiological concentrations of mutants impaired in this interaction should be unable to complement loss of $Mad2^{wt}$ (Figure 5A). To test this, we asked whether physiological concentrations of $Mad2^{R133A}$ and $Mad2^{R133E-Q134A}$ sustained the SAC in the absence of endogenous Mad2. For this, we knocked down the expression of Mad2 in HeLa cells by RNA interference (RNAi) and complemented its expression with RNAi-insensitive, HA-tagged $Mad2^{wt}$, $Mad2^{R133A}$, and $Mad2^{R133E-Q134A}$ alleles (Figure 5). Expression of endogenous Mad2 had substantially decreased after two rounds of transfection of a pSuper vector expressing a short hairpin targeting Mad2 [38]. In the meantime, the expression of RNAi insensitive alleles of Mad2 and its mutants from a pBabe vector cotransfected with pSuper had reached near physiological conditions (Figure 5B). As it was an essential precondition for this experiment, we tested the ability of the RNAi-insensitive alleles of Mad2 to bind Mad1. HA-$Mad2^{wt}$, HA-$Mad2^{R133A}$, and HA-$Mad2^{R133E-Q134A}$, but not $Mad2^{\Delta C}$, bound Mad1 after depletion of endogenous Mad2 (Figure 5C).

Being expressed at relatively low levels, none of the Mad2 alleles caused cell cycle arrest in the absence of nocodazole (Figure 5D, left). In the presence of nocodazole, control cells depleted of Mad2 failed to arrest in mitosis, showing that loss of Mad2 abrogates the SAC (Figure 5D, right, yellow bars). Complementation with RNAi-insensitive $Mad2^{wt}$ reestablished a significant level of mitotic arrest (red bars). As for analogous complementation experiments with BubR1 [39], we did not observe full recovery of checkpoint competence in cells expressing the RNAi-insensitive $Mad2^{wt}$ allele. A possible explanation is that the expression levels of HA-Mad2 complementing endogenous Mad2 are not completely stable, peaking at 40 hr after transfection and rapidly decreasing thereafter (not shown).

$Mad2^{R133A}$ and $Mad2^{R133E-Q134A}$ were completely impaired in complementing loss of Mad2 in nocodazole (Figure 5D, blue and violet bars). These alleles caused even lower counts of mitotic cells than in the absence of rescue constructs, suggesting an exacerbation of the checkpoint incompetence caused by loss of endogenous Mad2. Despite the imperfect levels of recovery obtained with $Mad2^{wt}$, these results confirm that the binding interface between O-Mad2 and C-Mad2 is essential to maintain the SAC at physiological protein concentrations. Of note, pCMV-driven overexpression of $Mad2^{R133A}$ effectively arrested cells in mitosis to an extent similar to that obtained with $Mad2^{wt}$ (not shown). High levels of Mad2 may drive formation of sufficient Mad2/Cdc20 by mass action, rendering the interaction of O-Mad2 with C-Mad2 dispensable. This interaction, however, is absolutely required at low Mad2 concentrations. Consistent with this, when moderately overex-

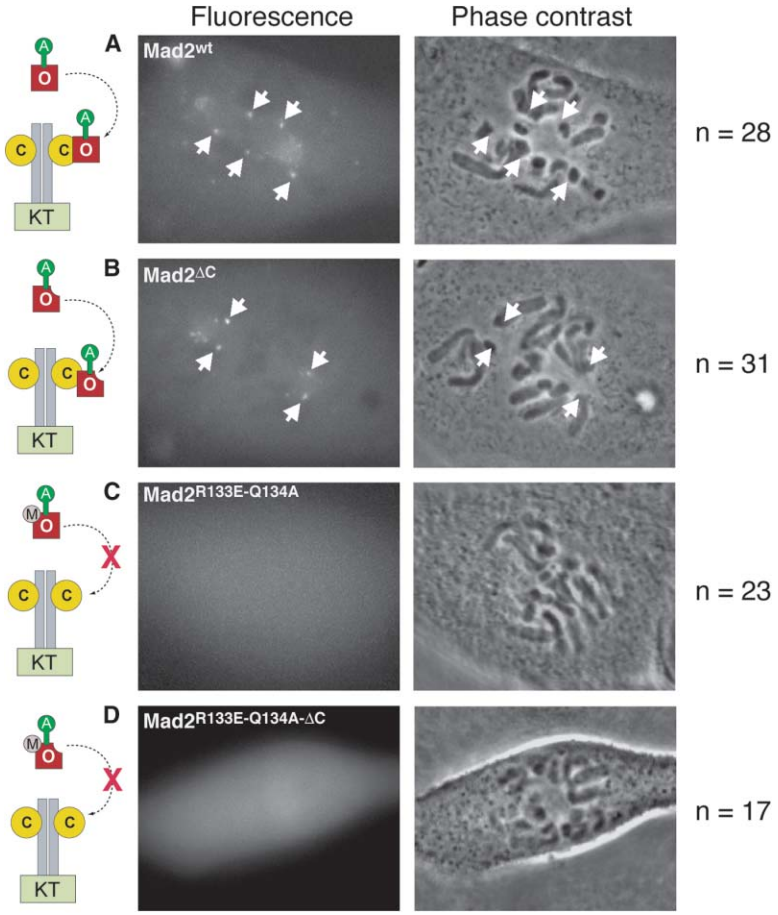

Figure 3. Localization of Wild-Type and Mutant Mad2 at the Kinetochore

PtK1 cells injected with Alexa-Mad2. For each panel, the fluorescence (left) and the phase contrast (right) images are shown. Images were acquired by taking a 13 plane/0.5 μm-step Z series through the sample. The images represent through focus projections of planes containing kinetochores. (A) Kinetochore localization of Mad2^{wt} with chromosomes that had not congressed to the spindle equator (arrow). (B) Positive staining at unattached kinetochores of cell injected with Alexa-Mad2$^{\Delta C}$. (C) Alexa-Mad2$^{R133E-Q134A}$ did not localize to the kinetochore. (D) Alexa-Mad2$^{\Delta C-R133E-Q134A}$ also failed to localize at the kinetochore.

pressed in *Xenopus* blastomeres, only Mad2^{wt}, but not Mad2^{R133}, promotes cell cycle arrest [40].

Discussion

Here, we propose a new model to describe the roles of Mad1 and Mad2 in the SAC, which we have named the "Mad2 template" model (Figure 6). This model can be broken down as follows: (1) two distinct conformers of Mad2 exist: O-Mad2, which predominates in the cytosol and accounts for the majority of Mad2, and C-Mad2, the conformation Mad2 adopts when bound to Mad1 or Cdc20; (2) Mad2 is recruited to kinetochores as O-Mad2, with the exception of that contained in the Mad1/Mad2 complex; (3) the O-Mad2 receptor at the kinetochore is Mad1/Mad2—Mad1 promotes kinetochore localization of Mad1/Mad2, and C-Mad2 contains the critical surface of the O-Mad2 receptor; (4) O-Mad2 and Mad1 bound C-Mad2 are distinct and nonexchanging within the timeframe of SAC activation; (5) the interaction with C-Mad2 facilitates binding of O-Mad2 to Cdc20; and (6) the Cdc20/C-Mad2 complex represents a structural copy of Mad1/C-Mad2 acting to promote further transformation of O-Mad2 into Cdc20 bound C-Mad2 away from kinetochores.

There is good evidence that C-Mad2 and O-Mad2 are stable conformations of Mad2 (point 1) [22, 28, 29, 31, 32]. O-Mad2 is the conformation of cytosolic Mad2 [32, 33]. It is possible that the O-Mad2 conformation is actively maintained in the cytoplasm to revert spontaneous formation of ligand-free C-Mad2. In HeLa cells, Mad2 exists predominantly as O-Mad2, but bacterially expressed Mad2 populates both conformations in the absence of Mad1 or Cdc20 [32, 33]. Spontaneous formation of empty C-Mad2 in vitro is not necessarily significant and not surprising when considering that the safety belt is designed to convert reversibly from O- to C-Mad2 and that empty C-Mad2 is stabilized by O-Mad2 in the Mad2^{wt} dimers.

Mad2 is recruited to kinetochores as O-Mad2 by the Mad1/C-Mad2 complex, and O-Mad2 and Mad1 bound C-Mad2 are distinct and nonexchanging (points 2–4). In this perspective, Mad1 and Cdc20 do not compete for Mad2 binding despite their related Mad2 binding motifs. The existence of Mad1-free and Mad1 bound pools of Mad2, corresponding to ~70% and ~30% of total Mad2, respectively, is well established, but it was unclear whether these pools exchanged Mad2 subunits at relevant rates [8, 9, 14, 15, 22, 24, 26, 32]. Several indications suggest that the two pools remain distinct: (1) recombinant Mad1/Mad2 is stable and does not release Mad2 in the presence of Cdc20 in vitro (Figure 1); (2) Mad2$^{R133E-Q134A}$, which binds Mad1, but not C-Mad2, fails to be recruited to kinetochores, suggesting that there are no C-Mad2 vacancies to be filled (Figure 3)—given the high turnover rate of Mad2 at the kinetochore [18,

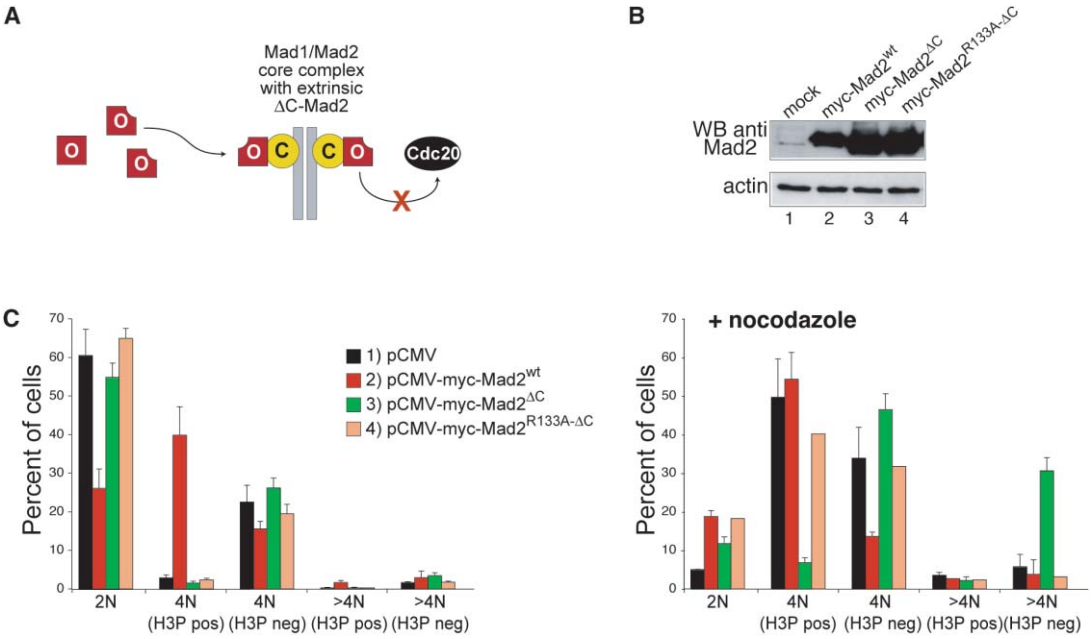

Figure 4. Functional Analysis of Mad2$^{\Delta C}$ in HeLa Cells

(A) Model for dominant-negative effect of Mad2$^{\Delta C}$. After binding Mad1/Mad2, Mad2$^{\Delta C}$ prevents kinetochore recruitment of O-Mad2^{wt} and formation of Mad2/Cdc20.

(B) Western blotting with an anti-Mad2 Ab of lysates of HeLa cells transfected with empty pCMV (lane 1) or pCMV expressing myc-Mad2^{wt} (lane 2), myc-Mad2$^{\Delta C}$ (lane 3), and myc-Mad2$^{R133A-\Delta C}$ (lane 4). Like Mad2$^{R133E-Q134A-\Delta C}$, this mutant does not bind the Mad1/Mad2 core [33].

(C) Left, 44–46 hr post transfection of the indicated constructs, HeLa cells were harvested, and DNA content and Ser10 phosphorylation of Histone H3 (H3P, a mitotic marker) was analyzed for myc-positive cells by three-color flow cytometry. Right, 26–28 hr post transfection of the indicated constructs, nocodazole was added to trigger the checkpoint. Cells were harvested after 18 hr and analyzed as above. Error bars represent standard deviations.

20, 21], if C-Mad2 core subunits were exchanging, we would expect significant kinetochore recruitment of Mad2$^{R133E-Q134A}$; (3) an immobile pool of Mad2 at mitotic kinetochores coexists with a high turnover mobile fraction of equal intensity [20]. Most likely, visualization of this immobile fraction was made possible by longer times of incorporation of fluorescent Mad2 into the Mad1/Mad2 core complex relative to other analyses [18, 21]. Given that Mad1 is immobile [20, 21], the nonrecovering fraction of Mad2 likely represents C-Mad2 in the Mad1/Mad2 complex.

We did not address how the interaction of O-Mad2 with Mad1/C-Mad2 facilitates binding of Mad2 to Cdc20 (point 5). All genetic and biochemical evidence shows that Mad2 binding to Cdc20 is Mad1 dependent [15, 22–25]. Because the role of Mad1 is to localize C-Mad2 at kinetochores, we propose that Mad1 bound C-Mad2 is also required to form Mad2/Cdc20. Indeed, the interaction of O-Mad2 with C-Mad2 is essential to maintain the checkpoint (Figures 5 and 6). The structural conversion of O-Mad2 into C-Mad2 bound to Cdc20 involves relatively large activation energies [22, 29, 32]. We suspect that the O-Mad2/C-Mad2 interaction accelerates this conversion during SAC activation. A structural investigation of the O-Mad2/C-Mad2 complex is underway and will hopefully shed light on how this conversion takes place. We are also investigating if and how the Mad1/Mad2 core complex directly affects the kinetics of Mad2 binding to Cdc20. Because the Mad2/Cdc20 interaction depends on Mad1 in living cells, appropriate conditions recreating this dependency in vitro must be identified. Furthermore, Cdc20 segments such as Cdc20$^{111-138}$ bind Mad2 more tightly than full-length Cdc20, and Cdc20 is also expected to undergo defined rearrangements to bind Mad2 [9, 35, 41]. These events may take place on a unique platform at the kinetochore, whose exact composition needs now to be unveiled. Addressing the role of the O-Mad2/C-Mad2 interaction directly with purified components is unlikely to yield insightful responses before more sophisticated in vitro assays are developed.

We postulate that the SAC starts when Mad1/Mad2 and O-Mad2 meet at the kinetochore near nuclear envelope breakdown. This enhances the transformation of O-Mad2 into Cdc20 bound C-Mad2 (Figure 6A). In the absence of stimulatory kinetochore function, the rate of formation of the MCC complex is insufficient to avoid anaphase prior to completion of kinetochore attachment. In this model, kinetochores accelerate the formation of the MCC, whereas its rate of disassembly remains relatively fast to allow rapid anaphase onset upon completion of bipolar attachment. This implies faster dissociation of Cdc20/Mad2 relative to Mad1/Mad2. For reasons discussed above, this is reasonable but will need to be reassessed with the MCC of which Cdc20/Mad2 is only a subcomplex.

Although we do not have a molecular description of this mechanism, our data indicate that C-Mad2 bound

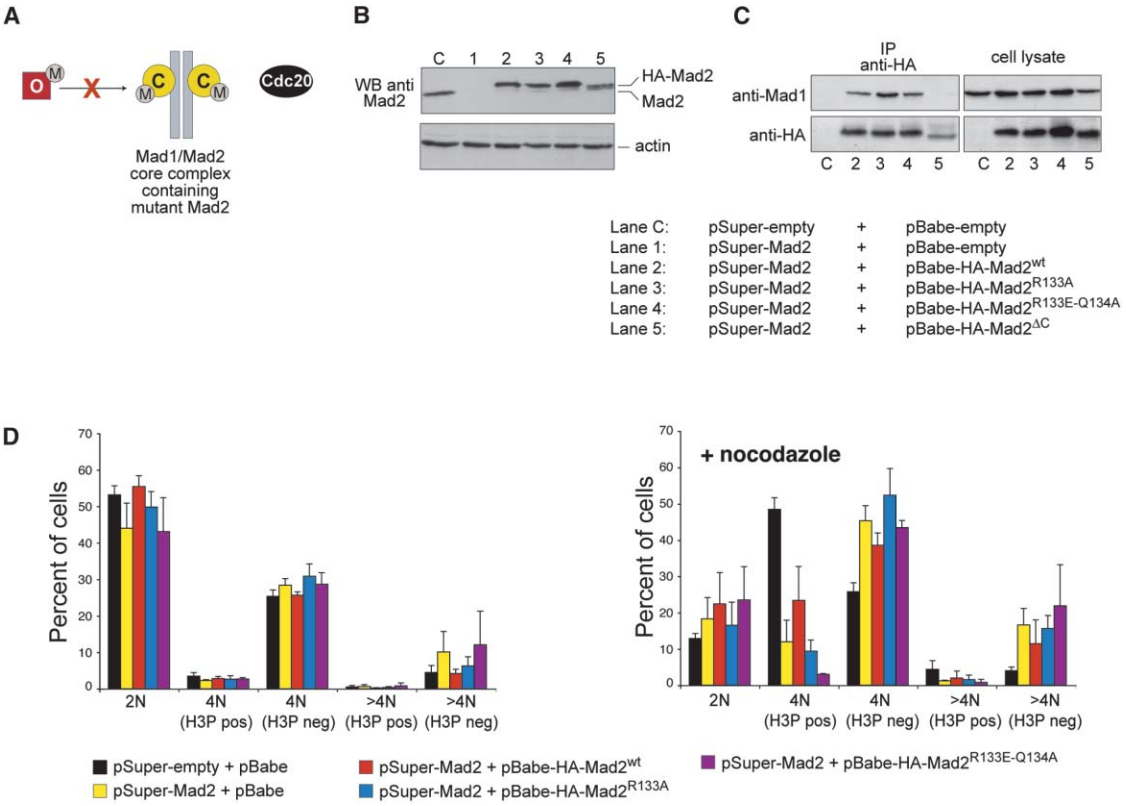

Figure 5. Functional Analysis of Mad2^{R133A} and Mad2$^{R133E-Q134A}$ in HeLa Cells

(A) Mad2^{R133A} and Mad2$^{R133E-Q134A}$ mutants are expected to be unable to sustain the SAC in the absence of Mad2^{wt}. Both mutants bind Mad1 as tightly as Mad2^{wt}. Because both mutants are impaired in O-Mad2/C-Mad2 binding, they cannot sustain the SAC.

(B) Mad2 expression in HeLa cells was silenced by RNAi (lane 1) with pSUPER-Mad2 [38]. Mad2^{wt} (lane 2), Mad2^{R133A} (lane 3), Mad2$^{R133E-Q134A}$ (lane 4), and Mad2$^{\Delta C}$ (lane 5) alleles made insensitive to RNAi with silent point mutations were expressed as HA-tag fusions from a pBabe vector cotransfected with pSUPER. HA-tagged Mad2 expressed from pBabe was detected with an anti-Mad2 antibody.

(C) HA-tagged Mad2 proteins enter a complex with Mad1, as shown by immunoprecipitation. Mad2$^{\Delta C}$ was the only allele that did not interact with Mad1 in the absence of endogenous Mad2.

(D) Left, flow cytometry of exponentially growing HeLa cells transfected with the indicated vectors. Right, cell cycle profiles of cells harvested 18 hr after adding nocodazole. Error bars represent standard deviations.

to Mad1 favors the transformation of O-Mad2 into C-Mad2 bound to Cdc20. This is reminiscent of the template-assisted conversion of prion proteins [42]. For sake of clarity, we are not proposing that Mad2 is a prion because differences with prions are heavier than similarities in this comparison. For instance, the transformation of Mad2 may be completely reversible and protein misfolding is unlikely to play a role in the regulation of Mad2. Furthermore, prions instate an inheritable state, whereas there is no evidence that Mad2 has such properties.

From a structural perspective, however, the parallel holds as it emphasizes a mechanism of homodimerization based on the selective interaction of different conformers of the same protein, ultimately resulting in the conversion of one into the other. The parallel is also conceptually useful as it suggests a mechanism for signal amplification in the SAC (point 6). Mad1 and Cdc20 share a similar Mad2 binding motif, and Mad2 adopts the C-Mad2 conformation within both complexes [22, 29]. In this respect, the C-Mad2/Mad1 and C-Mad2/Cdc20 complexes are structurally equivalent. Their relationship is one of template (C-Mad2/Mad1 core) and copy (C-Mad2/Cdc20). As a functional copy of C-Mad2/Mad1, C-Mad2/Cdc20 released in the cytoplasm might cause further conversion of O-Mad2 into C-Mad2/Cdc20. This speculation, which is contained in point 6 of the model, suggests that signal amplification in the SAC is caused by the C-Mad2-generating activities of kinetochore C-Mad2/Mad1 core and cytoplasmic C-Mad2/Cdc20 (Figure 6).

The characterization of p31^{comet} (previously known as CMT2) as a Mad2 ligand required to exit mitosis provides a strong indication in favor of this model [43]. As O-Mad2, also p31^{comet} recognizes selectively C-Mad2 in the Mad1/Mad2 and Cdc20/Mad2 complexes and fails to bind O-Mad2 [44] (R. Hagan et al., submitted). The "Mad2 template" model suggests that p31^{comet} hampers the transformation of O-Mad2 into C-Mad2 by competing with O-Mad2 for binding to C-Mad2/Mad1 and C-Mad2/Cdc20 (Figure 6B), a prediction that we are currently testing.

Conclusions

We show that Mad1/Mad2 is the kinetochore receptor for Mad2. The interaction of distinct Mad2 conformers is the core of the "Mad2 template" model and allows

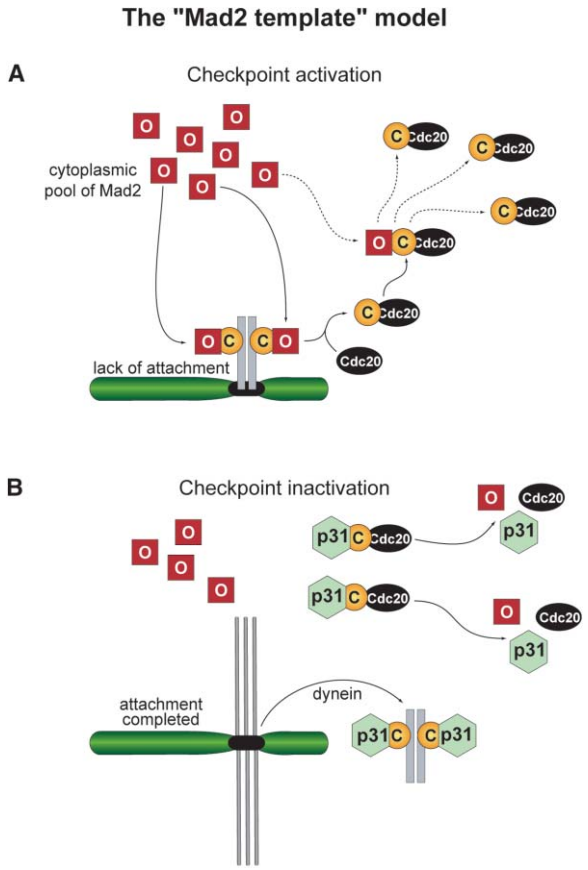

Figure 6. A New Model for the Spindle Checkpoint

(A) Encounter of O-Mad2 with C-Mad2 bound to Mad1 starts the SAC. The Mad1/Mad2 core complex recruits O-Mad2 to kinetochores, and O-Mad2 is converted into C-Mad2 bound to Cdc20. Mad2/Cdc20 is a structural copy of Mad1/Mad2 because Mad1 and Cdc20 share a Mad2 binding motif and Mad2 adopts the same C-Mad2 conformation in these complexes. The C-Mad2/Cdc20 complex dissociates from the Mad1/Mad2 core complex. In the cytosol, Mad2/Cdc20 acts as a structural equivalent of Mad1/Mad2 to convert more O-Mad2 into Cdc20 bound C-Mad2. Signal amplification occurs because Mad2/Cdc20 converts O-Mad2 to Cdc20 bound C-Mad2. Dashed arrows represent hypothetical steps related to the amplification of the SAC signal by Mad2/Cdc20.

(B) A "separator" protein between O-Mad2 and C-Mad2 inactivates the SAC. p31^{comet} binds C-Mad2 and prevents its interaction with O-Mad2. The encounter of O-Mad2 and C-Mad2 may require the temporary inactivation of p31^{comet}. The Mad1/Mad2 core complex is removed from the kinetochore by a dynein-dependent mechanism [45].

understanding the behavior of Mad2 in the SAC. The novelty of the model presented here is that it includes a mechanism for SAC signal amplification away from the kinetochore. Attempts to validate this model and to understand the interaction of Mad2/Cdc20 with other components of the SAC, such as Bub1, BubR1, and Bub3, are undergoing in our laboratories.

Experimental Procedures

Plasmids

pGEX-Mad1$^{523–550}$, pGEX-CDC20$^{111–138}$, and pCMV-mycMad2 were described [28]. pET43-Mad2/6His-Mad1$^{485–718}$ contains the coding sequence of human Mad2 separated from human 6His-Mad1$^{485–718}$ by a ribosome binding site. We generated pET43-6His-Mad2, pET43-6His-Mad2$^{R133A/Q134A}$, and pET43-6His-Mad2$^{\Delta C}$ by ligation into NdeI/EcoRI sites of pET43. The Mad2 coding sequence was ligated into BamHI of pBabe-HA-puro to obtain pBabe-HA-Mad2. Mutants were generated with QuikChange (Stratagene).

Expression, Purification, and Alexa Labeling of Proteins

Mad2/6His-Mad1$^{485–718}$ was expressed in *E.coli* BL21-c41(DE3). Mad2 was expressed at limiting levels with respect to 6His-Mad1. A stoichiometric core forms because excess 6His-Mad1 unbound to Mad2 is insoluble in *E. coli*. After affinity chromatography on Ni-NTA-agarose (Qiagen), the protein was purified by ion exchange and SEC on Superdex-200 in PBS. Mad2 proteins were expressed in *E. coli* BL21(DE3) and purified as described [28]. Proteins were labeled with Alexa-488 succimidyl ester dye (Molecular Probes, Inc.) as described [18] with final dye-to-protein ratio of ~2:1.

Microscopy

Culture of PtK1 cells, microinjection, digital imaging microscopy, and image analysis were previously described [18]. Early prometaphase cells were microinjected with about 1%–5% cell volume of Alexa-labeled Mad2 proteins at about 3 μM needle concentration. Cells were imaged on a Nikon TE300 inverted microscope equipped with a Nikon 100×/NA 1.4 Plan Apo phase objective and an Orca II ER cooled-CCD camera (Hamamatsu). Fluorescence was detected by using 2×2 binned images with 250 msec exposures.

Analytical SEC

Analytical SEC was carried out on a SMART device (Amersham-Pharmacia Biotech) with a Superdex-200 PC 3.2/30 column in PBS. 20 μM Mad2/6His-Mad1$^{485–718}$ complex was incubated for 1h at 20°C with 40 μM Alexa-Mad2 or Alexa-Mad2 mutants. The reactions were separated by SEC. Elution was carried out at 40 μl/min.

Cell Culture and Transfection

HeLa cells were grown in Dulbecco's modified Eagle medium (DMEM, Euroclone) supplemented with 10% bovine calf serum (Hyclone) and 2 mM L-glutamine. Growing HeLa cells were transfected with either a standard calcium phosphate precipitation procedure or lipofectamine reagent (Gibco-BRL). Nocodazole (Sigma) was used at 100 ng/ml. PtK1 cells were grown as described [18].

Antibodies

Anti-Mad2 (clone AS55-A12) and anti-Mad1 (clone BB3-8) monoclonals were obtained by immunizing Balb/C mice with the Mad2/Mad1$^{485–718}$ complex and produced at the IFOM-IEO campus monoclonal antibody facility; AC-40 anti-actin monoclonal was from Sigma; 16B12 anti-HA monoclonal and polyclonal anti-HA antibody were from BABCO; 9E10 anti-c-Myc monoclonal was from Oncogene; rabbit polyclonal anti-phospho-histone-H3 was from Upstate Biotechnology. Donkey anti-mouse or anti-rabbit IgG secondary antibodies conjugated to either FITC or Cy5 were from Jackson Laboratories, Inc.

Immunoprecipitations

HeLa cells were harvested by trypsinization and lysed in 50 mM Hepes (pH 7.5), 150 mM NaCl, 0.5% NP40, 1% glycerol, 5 mM EDTA, 10 mM Na_3VO_4, 50 mM NaF, 20 mM Na_4-pyrophosphate, 100 ng/ml leupeptine, 100 ng/ml Aprotinin, and 1 mM PMSF for 20 min on ice. Cell lysates were centrifuged for 15 min at 13,000 rpm at 4°C in an Eppendorf microcentrifuge. Protein amounts were measured with protein assay reagent (Bio-Rad Laboratories) as specified by the manufacturer, and equivalent amounts of total protein were used for immunoprecipitation. 0.4 mg of each cell lysate were incubated with 2 μg of rabbit polyclonal anti-HA antibody (BABCO) for 1 hr at 20°C followed by incubation with protein A Sepharose beads for 2 hr. The beads were washed three times in lysis buffer, eluted in SDS sample buffer, and analyzed by SDS-PAGE and Western blotting.

RNAi and Overexpression

HeLa cells (50% confluence) were cotransfected with calcium phosphate twice at 24 hr intervals with 8 μg pSUPER-Mad2 [38] and 10

μg of rescue constructs pBABE-HA-Mad2, pBABE-HA-Mad2^{R133A}, or pBABE-HA-Mad2$^{R133E-Q134A}$ containing silent mutations GAA_{169} and TCT_{170} in place of Mad2 codons GAG_{169} and TCG_{170}. 20–24 hr after second transfection, cells were split 1:3 to maintain log phase. 30–40 hr after second transfection, nocodazole was added (100 ng/ml). Cells were harvested 18–22 hr after adding nocodazole and treated for FACS. Samples were also lysed and analyzed by Western blotting. For overexpression, HeLa cells were grown to 70% confluence and transfected with 10 μg pCMV-mycMad2 (or Mad2 mutants) by using lipofectamine, and after 16–18 hr, cells were split 1:3. 26–28 hr after transfection, nocodazole was added. Cells were harvested 18 hr after nocodazole addition and treated for FACS analysis or WB.

Flow Cytometry

Cells were harvested by trypsinization and fixed with 1% formaldehyde and 75% ethanol. After fixation, cells were permeabilized with 0.1% Triton X-100 and stained with anti-phospho-histone-H3, anti-myc, or anti-HA antibodies. For DNA content, cells were treated with 5 μg/ml propidium iodide and 250 μg/ml RNaseA. Data acquisition and analysis were performed by using a FACSCalibur flow cytometer (Becton Dickinson) with CellQuest 3.3 software.

Supplemental Data

Supplemental Data include four figures and a table and can be found with this article online at http://www.current-biology.com/cgi/content/full/15/3/214/DC1/.

Acknowledgments

A.D.A. is an European Molecular Biology Organization postdoctoral fellow. A.M. is an EMBO Young Investigator and a Scholar of the Italian Foundation for Cancer Research (FIRC). This work was supported by the Italian Association for Cancer Research and the Human Frontier Science Program. We thank Rene Medema for the pSUPER-Mad2 vector; Marina Melixetian for pBABE-Mad2; Simonetta Piatti, Bruno Amati, Claudio Basilico, and the Musacchio group for discussions; and Sergio Bossi, Simona Ronzoni, Ivan Muradore, and Daniele Piccini for technical help.

Received: November 11, 2004
Revised: December 7, 2004
Accepted: December 7, 2004
Published: February 8, 2005

References

1. Musacchio, A., and Hardwick, K.G. (2002). The spindle checkpoint: structural insights into dynamic signalling. Nat. Rev. Mol. Cell Biol. *3*, 731–741.
2. Yu, H. (2002). Regulation of APC-Cdc20 by the spindle checkpoint. Curr. Opin. Cell Biol. *14*, 706–714.
3. Cleveland, D.W., Mao, Y., and Sullivan, K.F. (2003). Centromeres and kinetochores: from epigenetics to mitotic checkpoint signaling. Cell *112*, 407–421.
4. Nasmyth, K. (2002). Segregating sister genomes: the molecular biology of chromosome separation. Science *297*, 559–565.
5. Peters, J.M. (2002). The anaphase-promoting complex: proteolysis in mitosis and beyond. Mol. Cell *9*, 931–943.
6. Bharadwaj, R., and Yu, H. (2004). The spindle checkpoint, aneuploidy, and cancer. Oncogene *23*, 2016–2027.
7. Aravind, L., and Koonin, E.V. (1998). The HORMA domain: a common structural denominator in mitotic checkpoints, chromosome synapsis and DNA repair. Trends Biochem. Sci. *23*, 284–286.
8. Fang, G. (2002). Checkpoint protein BubR1 acts synergistically with Mad2 to inhibit anaphase-promoting complex. Mol. Biol. Cell *13*, 755–766.
9. Tang, Z., Bharadwaj, R., Li, B., and Yu, H. (2001). Mad2-independent inhibition of APC-Cdc20 by the mitotic checkpoint protein Bub1R. Dev. Cell *1*, 227–237.
10. Chen, R.-H. (2002). BubR1 is essential for kinetochore localization of other spindle checkpoint proteins and its phosphorylation requires Mad1. J. Cell Biol. *158*, 487–496.
11. Millband, D.N., and Hardwick, K.G. (2002). Fission yeast Mad3p is required for Mad2p to inhibit the anaphase-promoting complex and localizes to kinetochores in a Bub1p-, Bub3p-, and Mph1p-dependent manner. Mol. Cell. Biol. *22*, 2728–2742.
12. Shannon, K.B., Canman, J.C., and Salmon, E.D. (2002). Mad2 and BubR1 function in a single checkpoint pathway that responds to a loss of tension. Mol. Biol. Cell *13*, 3706–3719.
13. Meraldi, P., Draviam, V.M., and Sorger, P.K. (2004). Timing and checkpoints in the regulation of mitotic progression. Dev. Cell *7*, 45–60.
14. Sudakin, V., Chan, G.K., and Yen, T.J. (2001). Checkpoint inhibition of the APC/C in HeLa cells is mediated by a complex of BUBR1, BUB3, CDC20, and MAD2. J. Cell Biol. *154*, 925–936.
15. Fraschini, R., Beretta, A., Sironi, L., Musacchio, A., Lucchini, G., and Piatti, S. (2001). Bub3 interaction with Mad2, Mad3 and Cdc20 is mediated by WD40 repeats and does not require intact kinetochores. EMBO J. *20*, 6648–6659.
16. Hardwick, K.G., Johnston, R.C., Smith, D.L., and Murray, A.W. (2000). MAD3 encodes a novel component of the spindle checkpoint which interacts with Bub3p, Cdc20p, and Mad2p. J. Cell Biol. *148*, 871–882.
17. Gorbsky, G.J., Kallio, M., Daum, J.R., and Topper, L.M. (1999). Protein dynamics at the kinetochore: cell cycle regulation of the metaphase to anaphase transition. FASEB J. Suppl. *13*, S231–S234.
18. Howell, B.J., Hoffman, D.B., Fang, G., Murray, A.W., and Salmon, E.D. (2000). Visualization of Mad2 dynamics at kinetochores, along spindle fibers, and at spindle poles in living cells. J. Cell Biol. *150*, 1233–1250.
19. Kallio, M.J., Beardmore, V.A., Weinstein, J., and Gorbsky, G.J. (2002). Rapid microtubule-independent dynamics of Cdc20 at kinetochores and centrosomes in mammalian cells. J. Cell Biol. *158*, 841–847.
20. Shah, J.V., Botvinick, E., Bonday, Z., Furnari, F., Berns, M., and Cleveland, D.W. (2004). Dynamics of centromere and kinetochore proteins; implications for checkpoint signaling and silencing. Curr. Biol. *14*, 942–952.
21. Howell, B.J., Moree, B., Farrar, E.M., Stewart, S., Fang, G., and Salmon, E.D. (2004). Spindle checkpoint protein dynamics at kinetochores in living cells. Curr. Biol. *14*, 953–964.
22. Luo, X., Tang, Z., Rizo, J., and Yu, H. (2002). The Mad2 spindle checkpoint protein undergoes similar major conformational changes upon binding to either Mad1 or Cdc20. Mol. Cell *9*, 59–71.
23. Hwang, L.H., Lau, L.F., Smith, D.L., Mistrot, C.A., Hardwick, K.G., Hwang, E.S., Amon, A., and Murray, A.W. (1998). Budding yeast Cdc20: a target of the spindle checkpoint. Science *279*, 1041–1044.
24. Chung, E., and Chen, R.-H. (2002). Spindle checkpoint requires Mad1-bound and Mad1-free Mad2. Mol. Biol. Cell *13*, 1501–1511.
25. Martin-Lluesma, S., Stucke, V.M., and Nigg, E.A. (2002). Role of hec1 in spindle checkpoint signaling and kinetochore recruitment of mad1/mad2. Science *297*, 2267–2270.
26. Chen, R.H., Shevchenko, A., Mann, M., and Murray, A.W. (1998). Spindle checkpoint protein Xmad1 recruits Xmad2 to unattached kinetochores. J. Cell Biol. *143*, 283–295.
27. Chen, R.H., Brady, D.M., Smith, D., Murray, A.W., and Hardwick, K.G. (1999). The spindle checkpoint of budding yeast depends on a tight complex between the Mad1 and Mad2 proteins. Mol. Biol. Cell *10*, 2607–2618.
28. Sironi, L., Melixetian, M., Faretta, M., Prosperini, E., Helin, K., and Musacchio, A. (2001). Mad2 binding to Mad1 and Cdc20, rather than oligomerization, is required for the spindle checkpoint. EMBO J. *20*, 6371–6382.
29. Sironi, L., Mapelli, M., Knapp, S., Antoni, A.D., Jeang, K.-T., and Musacchio, A. (2002). Crystal structure of the tetrameric Mad1-Mad2 core complex: implications of a 'safety belt' binding mechanism for the spindle checkpoint. EMBO J. *21*, 2496–2506.
30. Waters, J.C., Chen, R.H., Murray, A.W., and Salmon, E.D. (1998). Localization of Mad2 to kinetochores depends on microtubule attachment, not tension. J. Cell Biol. *141*, 1181–1191.
31. Luo, X., Fang, G., Coldiron, M., Lin, Y., Yu, H., Kirschner, M.W., and Wagner, G. (2000). Structure of the mad2 spindle assembly

checkpoint protein and its interaction with cdc20. Nat. Struct. Biol. *7*, 224–229.

32. Luo, X., Tang, Z., Xia, G., Wassmann, K., Matsumoto, T., Rizo, J., and Yu, H. (2004). The Mad2 spindle checkpoint protein has two distinct natively folded states. Nat. Struct. Mol. Biol. *11*, 338–345.
33. De Antoni, A., Sala, V., and Musacchio, A. (2005). Explaining the oligomerization properties of the spindle checkpoint protein Mad2. Philos. Trans. R. Soc. Lond. B. Biol. Sci., in press.
34. Fang, G., Yu, H., and Kirschner, M.W. (1998). The checkpoint protein MAD2 and the mitotic regulator CDC20 form a ternary complex with the anaphase-promoting complex to control anaphase initiation. Genes Dev. *12*, 1871–1883.
35. Zhang, Y., and Lees, E. (2001). Identification of an overlapping binding domain on Cdc20 for Mad2 and anaphase-promoting complex: model for spindle checkpoint regulation. Mol. Cell. Biol. *21*, 5190–5199.
36. Canman, J.C., Salmon, E.D., and Fang, G. (2002). Inducing precocious anaphase in cultured mammalian cells. Cell Motil. Cytoskeleton *52*, 61–65.
37. Mikhailov, A., Cole, R.W., and Rieder, C.L. (2002). DNA damage during mitosis in human cells delays the metaphase/anaphase transition via the spindle-assembly checkpoint. Curr. Biol. *12*, 1797–1806.
38. Lens, S.M.A., Wolthuis, R.M.F., Klompmaker, R., Kauw, J., Agami, R., Brummelkamp, T., Kops, G., and Medema, R.H. (2003). Survivin is required for a sustained spindle checkpoint arrest in response to lack of tension. EMBO J. *22*, 2934–2947.
39. Kops, G.J., Foltz, D.R., and Cleveland, D.W. (2004). Lethality to human cancer cells through massive chromosome loss by inhibition of the mitotic checkpoint. Proc. Natl. Acad. Sci. USA *101*, 8699–8704.
40. Tunquist, B.J., Eyers, P.A., Chen, L.G., Lewellyn, A.L., and Maller, J.L. (2003). Spindle checkpoint proteins Mad1 and Mad2 are required for cytostatic factor-mediated metaphase arrest. J. Cell Biol. *163*, 1231–1242.
41. Camasses, A., Bogdanova, A., Shevchenko, A., and Zachariae, W. (2003). The CCT chaperonin promotes activation of the anaphase-promoting complex through the generation of functional Cdc20. Mol. Cell *12*, 87–100.
42. Aguzzi, A., and Haass, C. (2003). Games played by rogue proteins in prion disorders and Alzheimer's disease. Science *302*, 814–818.
43. Habu, T., Kim, S.H., Weinstein, J., and Matsumoto, T. (2002). Identification of a MAD2-binding protein, CMT2, and its role in mitosis. EMBO J. *21*, 6419–6428.
44. Xia, G., Luo, X., Habu, T., Rizo, J., Matsumoto, T., and Yu, H. (2004). Conformation-specific binding of p31(comet) antagonizes the function of Mad2 in the spindle checkpoint. EMBO J. *23*, 3133–3143.
45. Howell, B.J., McEwen, B.F., Canman, J.C., Hoffman, D.B., Farrar, E.M., Rieder, C.L., and Salmon, E.D. (2001). Cytoplasmic dynein/dynactin drives kinetochore protein transport to the spindle poles and has a role in mitotic spindle checkpoint inactivation. J. Cell Biol. *155*, 1159–1172.